A COMPUTER-ASSISTED STUDY OF RED CORAL POPULATION DYNAMICS

SAYOMI KAMIMOTO, HYE KYUNG KIM, EVELYN SANDER, AND THOMAS WANNER

ABSTRACT. We consider a 13-dimensional age-structured discrete red coral population model varying with respect to a fitness parameter. Our numerical results give a bifurcation diagram of both equilibria and stable invariant curves of orbits. We observe that not only for low levels of fitness, but also for high levels of fitness, populations are extremely vulnerable, in that they spend long time periods near extinction. We then use computer-assisted proofs techniques to rigorously validate the set of regular and bifurcation fixed points that have been found numerically.

1. INTRODUCTION

Coral plays an important role in the marine ecosystem, and coral reefs provide habitats to many sea animals and protect coastlines from breaking waves and storms. Red coral is a long-lived, slow-growing species, dwelling on Mediterranean rocky bottoms. Red coral populations are at risk due to both global climate change and overharvesting [4]. Bramanti, Iannelli, and Santangelo [3, 17] investigated red coral populations by scraping samples off the coast of Italy in Calafuria in the Western Ligurian Sea (43°30′ N, 10°20′ E, Italy, at a depth between 20 and 45m depth) and observing their growth rate over a four-year period. They used this data to construct a Leslie-Lewis transition matrix, a static life table, and a 13-dimensional dynamical population model. Using this model, they studied population trends by comparing small young colonies and bigger older colonies. However, they only considered a small range of population trends. In the current paper, we present a systematic study of this coral population model, shedding light on the long-term dynamics of the red coral populations. We can see the long-term effect of change in reproduction fitness. We establish the equilibrium structure and bifurcation points for the model, find a set of stable periodic invariant cycles, and show that for a large range of reproduction fitness these cycles get close to population extinction.

In addition to these observations, we present and implement methods which allow us to rigorously validate the model's equilibrium and bifurcation structure, including both a saddle-node and a Neimark-Sacker bifurcation. These validations use a modification of the Newton-Kantorovitch type method developed in [15, 19, 20].

FIGURE 1. Photographs of red coral colonies. The individual polyps
are visible particularly in the right-hand image. Photos from [1, 8].

While the previous version of this method merely used natural continuation, this
paper contains an extension of these results in which we consider rigorous validation
using pseudo-arclength continuation [9, 10]. In addition, we use computer-assisted
proof methods to prove the existence of saddle-node and Neimark-Sacker bifurcation
points on the equilibrium branch. These methods significantly extend the range of
applications of the constructive implicit function theorem which was introduced
in [15]. While for the purposes of this paper we restrict ourselves to the case of
finite-dimensional Euclidean spaces, the results can easily be adapted to the general
Banach space setting, with little change. Thus, the pseudo-arclength results can be
used for example in the setting of partial differenial equations, such as the setting
described in [16]. In other words, the present paper presents a functional analytic
foundation for using pseudo-arclength continuation in the context of computer-
assisted proofs based on the constructive implicit function theorem presented in [15].

The remainder of this paper is organized as follows. We introduce the age-based
red coral model in Section 2. In addition, we present a bifurcation diagram of fixed
points and stability of the model, along with a detailed discussion of oscillations.
These results show how even at high fitness levels, the oscillations lead to extreme
vulnerability of the population. Section 3 contains a functional-analytic approach
to the rigorous validation of the regular branches in the bifurcation diagram, which
is based on a constructive version of the implicit function theorem. Subsequently,
Section 4 details the validation for the three bifurcation points on the main fixed
point branch; namely, the saddle-node bifurcation in 4.2, the Neimark-Sacker bifur-
cation in 4.1, and the transcritical bifurction in 4.3. Section 5 contains conclusions
and future work.

2. Red coral population model

In this section we present the red coral population model of Bramanti, Iannelli,
and Santangelo [3, 17], based on their experimental and field data and a Leslie-Lewis
transition matrix. In addition, we describe the dynamics of the model in terms of
its bifurcation structure and discuss its implications.

2.1. **Description of the model.** A coral population is a self-seeding independent
group consisting of *polyps*, tiny soft-bodied organisms related to jellyfish. Polyps
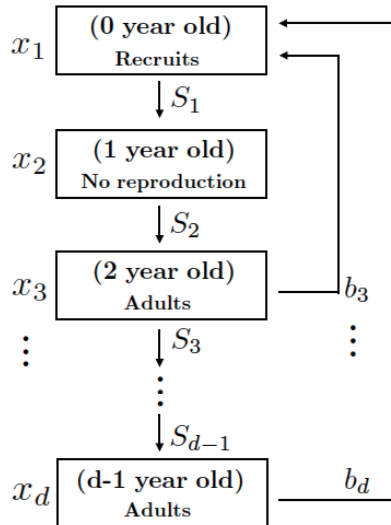
FIGURE 2. Life cycle of the coral population

form into *colonies*, which are distinct clusters with polyps residing on a surface, as shown in Figure 1. A polyp is born to a parent colony in a free-swimming larval stage. At the end of the larval stage, the polyp permanently attaches itself to a colony and cannot move again. The age of a colony has implications in terms of its size and polyp density. As a result, colony age determines the polyp attachment rate, the larval birth rate, and the polyp survival rate. Based on these factors, larvae will attach either to an existing colony or, especially if there is a high polyp density, *recruitment* will occur. That is, larvae do not attach to existing colonies, but instead form new colonies. Red coral polyps can reproduce larvae starting two years after their birth, implying that there is no birth in a colony less than two years old, since none of the polyps are old enough to reproduce. Reproduction occurs at a discrete time in summer, implying that a discrete population model is a natural modeling assumption.

Based on the setting above, rather than modeling the total large number of polyps in a coral population, the age-based model is a discrete time model for $(x_1, x_2, \ldots, x_d)$, where x_k is the number of colonies of age group k. The value d is the oldest colony in the population. While in principle this d could be large, in the observations made there was no colony of age group greater than 13. The value of x_k changes with respect to time (in years), where x_k^n denotes the number of colonies of age group k at year n. The colony life cycle is displayed in the schematic diagram shown in Figure 2. The downward arrows in Figure 2 indicate that x_{k+1}, the number of colonies in age group $k + 1$, is determined exclusively by the number of colonies in age group k in the previous year. This relation is linear with respect to population, with the survival rate constant S_k, i.e., we have $x_{k+1}^n = S_k x_k^{n-1}$. The survival rate values are determined by observation, and are given in Table 1, based on [17, Table 2].

Class k	Survival rate S_k	Fertility F_k
1	0.89	0
2	0.63	0
3	0.70	0.36
4	0.52	0.64
5	0.44	0.82
6	0.29	0.97
7	0.57	0.98
8	0.33	0.99
9	0.75	1
10	1	1
11	0.33	1
12	1	1
13		1

TABLE 1. Observational red coral data from [17]. Our calculations are based on their fitting functions given in (2.1) and (2.2), which were established using this data.

The upward arrows Figure 2 indicate that recruits may be larvae from any colony of age two or greater. Though it is not obvious from the schematic diagram, the recruitment rate is not linear, and it depends on both the total number of polyps in the colonies, as well as on the larvae birth rates. Considering that the base variables x_k denote the number of colonies in age group k, the total number of polyps can be deduced from the numbers p_k of polyps per colony in a colony of age group k, and the birth rates b_k depend on the fertility rates F_k given in Table 1. Combined with the observational data in [3], Bramanti et al. have then derived empirical expressions for the polyp per colony numbers p_k and the birth rates b_k, which are given by

$$(2.1) \qquad p_k = 1.239\, k^{2.324} \qquad \text{and} \qquad b_k = F_k\, k^{2.324}\,.$$

For our calculations in the present paper, we use these fitting functions rather than the original data, in keeping with the equations in [3]. In addition to the birth rates, the number of recruits x_1 depends also on a nonlinear function ϕ, which in turn depends on the density of polyps per unit area. This function ϕ is given by

$$(2.2) \qquad \phi(y) = \frac{c_1 e^{-\alpha y}}{y^2 + c_2 e^{-\beta y}}, \quad \text{with} \quad c_1 = 1.8 \cdot 10^5,\ c_2 = 1.3 \cdot 10^7,$$
$$\alpha = 5 \cdot 10^{-4},\ \beta = 3.4 \cdot 10^{-3}\,,$$

which again is a fit for the observational data in [3]. The shape of this nonlinearity is depicted in Figure 3. For a small density of polyps, the function ϕ increases with polyp density, whereas too large of a polyp density inhibits the creation of new colonies due to competition for resources.

We now explain how to compute the polyp population density P. We have already seen that the numbers p_k of polyps per colony in a colony of age group k satisfy the
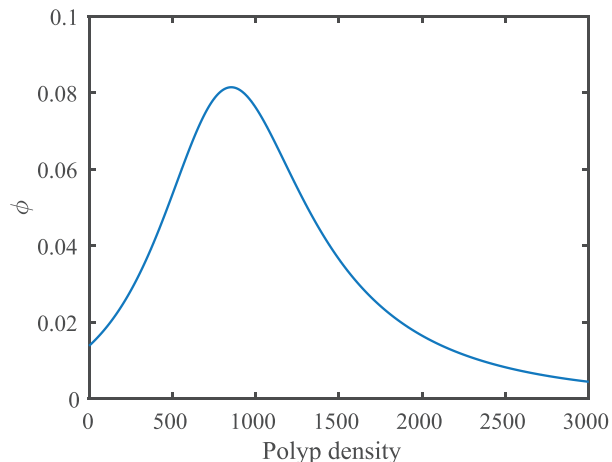
FIGURE 3. The recruits-to-larvae ratio function ϕ plotted with respect to polyp density P.

empirical formulas in (2.1). Thus, the total number of polyps in age group k is given by $p_k x_k$. Now let Ω denote the total area of the population site, which was measured to be equal to 36 dm^2 in [3]. Moreover, let $x = (x_1, x_2, \ldots, x_d)$ be a column vector giving the number of colonies of each age group, and let $p = (p_1, p_2, \ldots, p_d)$ denote the vector of polyps per colony in each age group. Then the total number of polyps in the (non-recruit!) population Q and the polyp population density P satisfy the identities

$$(2.3) \qquad Q = \sum_{k=2}^{d} p_k x_k \qquad \text{and} \qquad P = \frac{Q}{\Omega} \ .$$

Based on these preliminaries, let $x^n = (x_1^n, x_2^n, \ldots, x_d^n)$ represent the vector containing the number of colonies at year n, and let P be the polyp population density defined in (2.3). If we now define

$$(2.4) \qquad L(\lambda, x) = \begin{bmatrix} \lambda b_1 \phi(P) & \lambda b_2 \phi(P) & \ldots & \lambda b_{d-1} \phi(P) & \lambda b_d \phi(P) \\ S_1 & 0 & \ldots & 0 & 0 \\ 0 & \ddots & \ddots & & \vdots \\ \vdots & \ddots & \ddots & 0 & \vdots \\ 0 & \ldots & 0 & S_{d-1} & 0 \end{bmatrix} ,$$

where the bifurcation parameter λ is described below, then our model is given by

$$(2.5) \qquad x^{n+1} = L(\lambda, x^n) x^n \ .$$

The model (2.4) and (2.5) is an age-structured, nonlinear, discrete-time dynamical model. For the parameter value $\lambda = 1$, it is precisely based on the observational data in [3]. The nonlinearity arises only in the evolution of the variable x_1, which describes the number of recruit colonies. In a slight reformatting of notation, let the function $f : \mathbb{R} \times \mathbb{R}^d \to \mathbb{R}^d$ be given by $f(\lambda, x) = L(\lambda, x)x$. Then $x^{n+1} = f(\lambda, x^n)$,

meaning that the dynamical population variation corresponds to the iteration of the parameter-dependent nonlinear map f.

We still have to justify the introduction of the bifurcation parameter λ in the above formulas. Previous work concentrated on the effect of varying the biologically relevant reproductive number R, the total number of larvae produced by a single colony during its life span. This parameter is directly proportional to λ, as we will show in Section 2.3. The birth rate parameters b_k in the above equation are determined by observation of a specific coral population over a small time period. In order to consider a population model in which the population is placed under stress, such as in the case of climate change, it is necessary to change the parameters beyond what has been observed. While we could also consider modification of other parameters, we choose to follow along the lines of [3] and vary the birth rates, making the assumption that every birth rate parameter will be equally affected. Therefore, in our subsequent analysis, for every k we let the birth rate be given by λb_k, a fixed scaling factor compared to the originally observed birth rate.

2.2. **Fixed points of the coral population model.** We now consider the set of fixed points for the coral population model, given by the nonlinear function f defined above, and how this set changes as a function of the parameter λ. That is, we wish to determine the set of all pairs $(\lambda, x) \in \mathbb{R} \times \mathbb{R}^d$ such that $f(\lambda, x) = x$. As it turns out, this can be reformulated equivalently as a one-dimensional problem. To see this, assume that we have $x = f(\lambda, x)$. Then for all indices $k = 1, \ldots, d-1$ one has $x_{k+1} = S_k x_k$. Using these statements iteratively, one readily obtains

$$x_2 = S_1 x_1 , \quad x_3 = S_2 S_1 x_1 , \quad \ldots \quad x_d = S_{d-1} \cdots S_2 S_1 x_1 .$$

Thus, for all $k = 2, \ldots, d$ we have $x_k = a_k x_1$, where one uses the abbreviation

$$(2.6) \qquad\qquad a_k = \prod_{i=1}^{k-1} S_i ,$$

and we further define $a_1 = 1$ then one also has $x_1 = a_1 x_1$. Since we can write each component x_k for $k \geq 2$ as a function of x_1 alone, the fixed point problem is a one-dimensional problem, which is only a matter of determining x_1. Recall that we defined the polyp population density P in (2.3), and let $b = (b_1, b_2, \ldots, b_d)$. Then the equation for x_1 is given by

$$x_1 = \lambda (b \cdot x) \, \phi(P) .$$

Moreover, let $a = (a_1, a_2, \ldots, a_d)$. This immediately implies the identities

$$x = x_1 a , \qquad P = \frac{x_1}{\Omega} \sum_{k=2}^{d} p_k a_k , \qquad \text{and} \qquad b \cdot x = (b \cdot a) \, x_1 .$$

Altogether, this shows that a vector $x = (x_1, \ldots, x_d)$ is a fixed point for the map $f(\lambda, \cdot)$ if and only if $x = x_1 a$ and its first component x_1 satisfies the nonlinear equation

$$(2.7) \qquad\qquad x_1 = \lambda \, (b \cdot a) \, x_1 \, \phi \left(\frac{x_1}{\Omega} \sum_{k=2}^{d} p_k a_k \right) .$$

From this equation, one can then determine all fixed points of the coral population model. Notice that we clearly have the trivial solution $x = 0$ for all values of the parameter λ, which corresponds to an extinct population.

2.3. **The basic reproduction number.** An important biological parameter for the coral population is the total number of larvae produced by a single colony in its entire life span. This number only depends on the birth and survival rates, and one can easily see that it is given by

$$(2.8) \qquad R = \lambda b_1 + \lambda b_2 S_1 + \lambda b_3 S_2 S_1 + \cdots + \lambda b_d S_{d-1} S_{d-2} \ldots S_1 = \lambda \sum_{i=1}^{d} a_i b_i \ .$$

The number R is called the *basic reproduction number*. Using the notation from the last subsection, the above equation can be rewritten as

$$(2.9) \qquad\qquad\qquad\qquad R = (b \cdot a)\lambda \ .$$

In particular, while it is possible to vary R in such a way that the relationship between the birth rate constants vary, under our assumptions, the vectors b and a are fixed constant vectors, and we therefore have a fixed linear relationship between R and λ. To make it easy to compare our results with those of previous papers, we have chosen to plot all bifurcation diagrams with respect to the basic reproduction number R.

2.4. **The fixed point bifurcation diagram.** We now turn our attention to a description of the bifurcation diagram of the fixed points for the coral population system. This diagram is shown in Figure 4, where the set of fixed points is plotted in terms of the reproductive number R versus polyp population density P. The color in the diagram depicts the stability of the fixed points, and the diagram indicates the existence of three bifurcation points: a saddle-node and a Neimark-Sacker bifurcation on the nontrivial branch, which itself bifurcates from the trivial branch at a transcritical bifurcation. While subsequent sections of this paper will be used to verify the bifurcation diagram using computer-assisted proofs, the remainder of the current subsection is devoted to the discussion of dynamical aspects which are observed through numerical simulations.

Throughout our computations, we used the case of $d = 13$ age groups. The bifurcation diagram in Figure 4 was computed using a numerical continuation method starting at reproduction number $R = 300$, and allowing R to decrease. There appears to be a saddle-node point for $R \approx 12.28$ (which corresponds to $\lambda \approx 0.4213$), after which the basic reproduction number R of the fixed points begins to increase again. In Section 4 we use a computer-assisted proof to rigorously validate this saddle-node bifurcation point. The curve continues further until the population density reaches zero, which corresponds to an extinct population. We will see later that the extinction point can be found explicitly, and that it occurs at $R \approx 72.22$ (which corresponds to $\lambda \approx 2.478$). Moreover, the stability of the trivial solution $x = 0$ can readily be determined from the Jacobian matrix of f at the origin, and this shows that the extinction fixed point is stable for small R, corresponding to low fitness, and unstable for all larger values of the basic reproduction number R, with instability index 1. The bifurcation between the extinction fixed point being stable
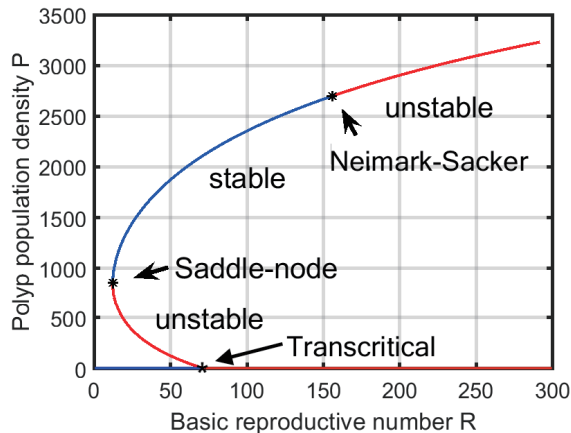
FIGURE 4. The bifurcation diagram of polyp density P as a function of the reproductive number R. While the diagram covers the range $R \in (12, 300)$, the birth rate data collected by Bramanti et al. in [3] are for $R \approx 29$.

and unstable occurs at the transcritical bifurcation point. All of these statements will be established rigorously in Section 4, including the appearance of the transcritical bifurcation point. Unlike the other two bifurcation points, no computer-assisted proofs are necessary along the trivial solution.

As mentioned before, the stability of the fixed points $x^* \in \mathbb{R}^{13}$ is indicated by color, with blue indicating stable fixed points and red representing unstable ones. The local stability at each fixed point in Figure 4 is determined numerically, based on whether all the eigenvalues of the Jacobian matrix $D_x f(\lambda, x)$ lie inside the unit circle or not. In the bifurcation diagram, we have not distinguished the index of the stability. If at least one of the eigenvalues lies outside the complex unit circle, then the fixed point is colored red, meaning unstable.

2.5. **Oscillations.** Figure 4 only shows the existence and stability behavior of fixed point solutions. But what about the dynamical behavior of the system? In this last subsection of Section 2, we focus on dynamical aspects of the model, in particular its oscillatory behavior on attracting invariant circles that form as a result of the Neimark-Sacker bifurcation. For a fixed parameter value $R > 154.1$ and for a typical initial condition, solutions converge to these invariant circles, and therefore the age-structured coral populations oscillate as time varies.

Figure 5 shows the dynamics of initial populations near fixed points, starting at a variety of different parameters and different initial aged-structured population vectors $y \in \mathbb{R}^{13}$. At reproduction number $R = 8.744$ (which corresponds to $\lambda = 0.3$), the solutions converge to the stable fixed point zero, i.e., the point of extinction. For $R = 29.15$ (corresponding to $\lambda = 1$), if we start at initial conditions ranging roughly from $0.15y$ to $2y$, where y is a vector of age-structured initial number of colonies which was chosen with polyp population density $P = 1500$, then solutions converge to a nontrivial stable fixed point. There is also an unstable fixed point denoted by
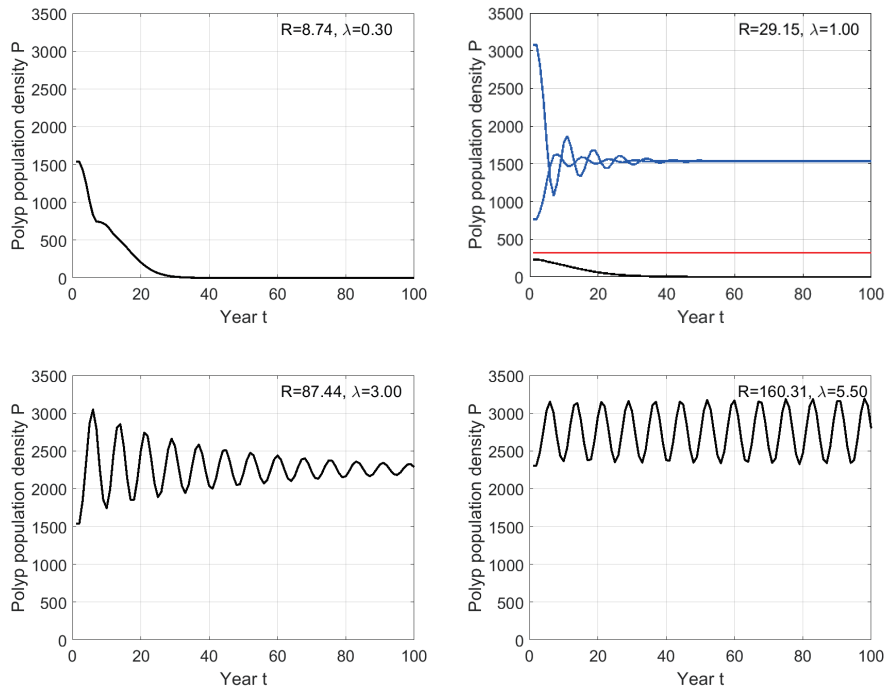
FIGURE 5. Dynamical behavior of some sample orbits of the red coral population model. All of these figures show the temporal evolution of the polyp population density P, and they are simulated over a time frame of 100 years each, at various parameter values.

the red line. In addition, one can observe bistability at this parameter value. If we start at a smaller value of P, such as for example at initial populations with polyp population density smaller than $0.15y$, solutions converge to zero, i.e., the coral population becomes extinct. At the basic reproduction number $R = 87.4437$ ($\lambda = 3$), though it takes longer time than 100 years, the solutions still converge to a stable nontrivial fixed point. In contrast, at $R = 160.31$ ($\lambda = 5.5$), population starting at $P = 1.5y$ oscillate. We used connected lines to show these oscillations more effectively, but recall that the map is in fact discrete.

The oscillations seen in the lower right subplot of Figure 5 form as a result of the Neimark-Sacker bifurcation. The fixed point stability switches from stable to unstable, and an invariant circle gains stability. Trajectories with initial conditions near fixed points but after the bifurcation are displayed in Figure 6. Perturbations around an unstable fixed point are repelled from the fixed point after the bifurcation, converging to an invariant closed curve. As the parameters R and λ increase, the size of the closed curve also increases, and the minimum population of a curve approaches the extinction point at the origin. That is, red coral populations become vulnerable at a large reproduction number, and a very small perturbation of the population would endanger the survival of the population despite the existing long recovery cycle.
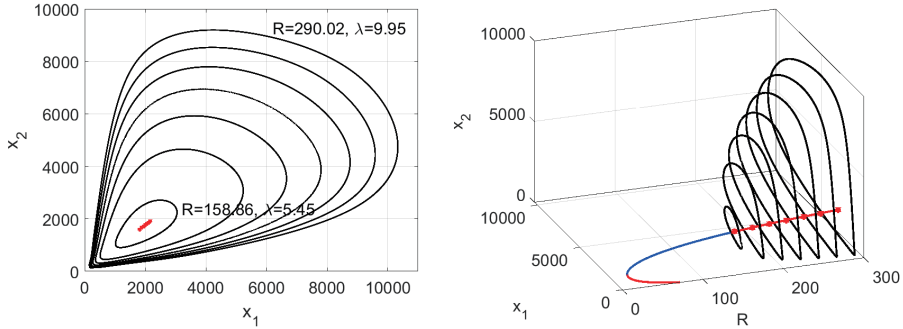
FIGURE 6. After the Neimark-Sacker bifurcation, oscillating orbits appear. After removing transients in the orbit, the orbit lies on an invariant closed curve. On the left, we plot the x_1- and x_2-components of these limit cycles. As the parameter R increases, the size of the closed curve increases. For large values of R, the coral population is close to the extinction point at the origin. On the right, the same orbits are shown with respect to R, along with the corresponding unstable fixed points at the same parameter value.
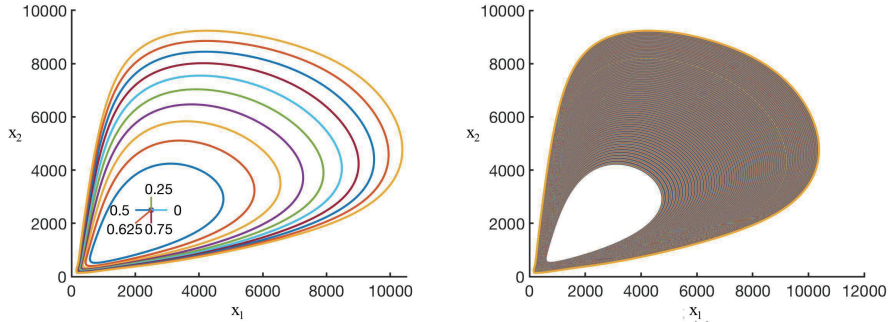

FIGURE 7. Invariant cycles for ten (left) and 500 (right) different parameter values. Even though we are guaranteed that some of the cycles contain stable periodic orbits, the periods are sufficiently high and the parameter ranges for which they exist are sufficiently small that it is hard to see them even in a close zoom (not depicted). Each orbit was computed using 100,000 iterates.

In order to better understand the stable invariant limit cycles that form after bifurcation, we have computed the rotation number, meaning the average angle of rotation per iterate, as a function of the parameter R. Specifically, we used the projection to the x_1x_2-plane to compute the rotation numbers. Our computations are performed using the weighted Birkhoff average method described in [7]. Figure 7 shows cycles at ten distinct parameter values on the left, and for 500 distinct parameters on the right. The corresponding rotation numbers are shown in Figure 8. The values are angles, but they are rescaled to have values in the range $(0, 1)$.
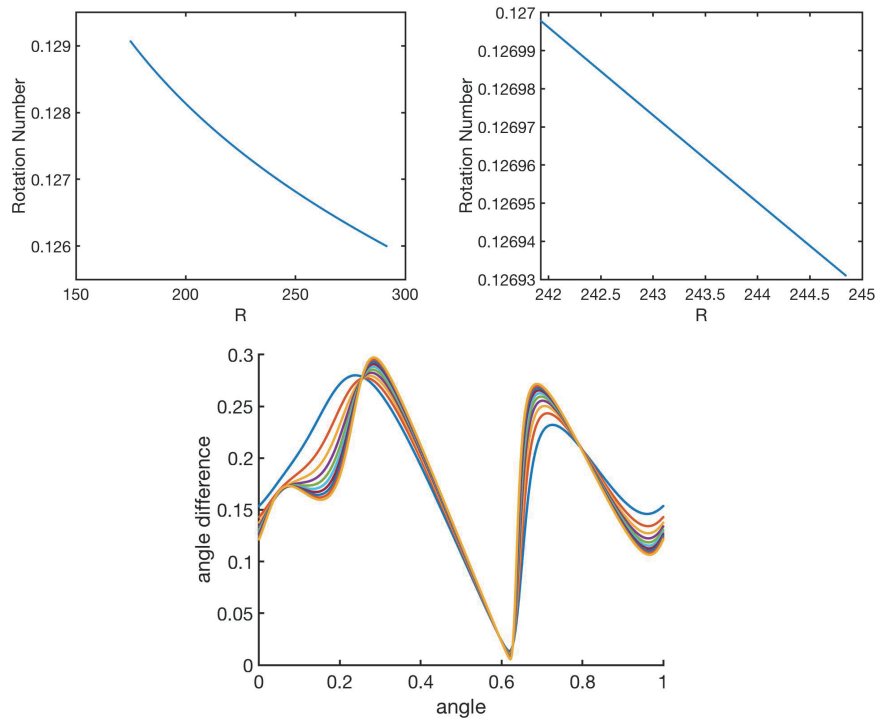
FIGURE 8.   The rotation number for the cycles shown in Figure 7
(top left) and a close up view of the rotation numbers (top right),
this time with one million iterates. The periodic orbits are of such
high periods that we cannot detect the devil's staircase type be-
havior of the rotation number within the Arnold tongue locking re-
gions. The rotation number is computed using the angle difference
between successive values of (x_1, x_2), computed with respect to the
point $(x_1, x_2) = (2500, 2500)$, and the angle versus angle difference
is depicted here (bottom) for the cycles for ten different R values.
The minimum occurs at the angle pointing towards the extinction
point.

Each rotation number was computed by considering the angle difference between
successive iterates when measured with respect to the point $(2500, 2500)$. To verify
our numerics and check that we have used a sufficient number of iterates in our
calculation, we compared the rotation number computed with 50,000 iterates to the
rotation number computed with 40,000 for a series of test parameters. In these test
parameters, the answer differs by 10^{-15} or less.

Note that we would expect to see a devil's staircase in the rotation numbers at the
parameter values when there are periodic orbits, but what we see looks smooth even
when quite zoomed in. This is due to the fact that the periodic orbits are extremely
high period. In particular, we are able to use a Farey tree calculation to find the
smallest denominator, corresponding to the lowest period, of a periodic orbit for
the case of a rational rotation number for this range of rotation numbers, using the

method in [2, 14]. In particular, we find that the lowest denominator in the range
[0.126, 0.129] is 39 (fraction 5/39). Not only is the lowest possible period quite large
and therefore hard to distinguish from a limit cycle, but also the large periodicity
implies that the Arnold tongue locking regions are very small parameter ranges,
meaning that we are not able to resolve them without more delicate computations.

The average rotation number gives only the mean of how much the population
is changing with respect to time. This leaves out some information as to how the
change in population depends on the location of the population. In the bottom
subplot in Figure 8, we show the angle difference as a function of the angle for
ten different values of R. That is, for each point in the invariant circle, we graph
how much the population is changing in one iterate (corresponding to one year) at
each point in the invariant circle. The smallest angle difference, corresponding to
the slowest change, occurs for angle ≈ 0.625, corresponding to the values closest to
the origin extinction point. Therefore, a portion of the invariant circles is getting
dangerously close to the origin, such that a small perturbation could result in the
extinction of the whole coral population. To compound matters further, the orbits
are staying near the extinction point for longer than they remain in any other region,
since at these points the observed angle differences are very close to zero. Thus the
population remains extremely vulnerable for a particularly long time.

3. Branch validation and continuation

We now turn to the rigorous validation of fixed points, both for regular and
bifurcation values. Our general approach is the constructive implicit function the-
orem from [15]. This is a rigorous result that combines with a numerical interval
arithmetic calculation to give rise to a validated method for finding a branch in the
zero set of a function which depends on a single parameter. In the following four
subsections, we will first recall the constructive implicit function theorem, and then
define an extended system which can be used for pseudo-arclength continuation.
After that, we prove two results which form the basis of our approach, and describe
the necessary preconditioning for the coral population model application.

3.1. **The constructive implicit function theorem.** Before stating the full re-
sult, here is a summary. Given an approximate zero (α^*, x^*) of a function $G(\alpha, x)$
where x is contained in a Banach space and $\alpha \in \mathbb{R}$, under certain hypotheses on
G and its derivatives evaluated at the approximate zero (α^*, x^*), combined with
Lipschitz estimates near this point, there exist two regions in parameter and phase
space. First, the *accuracy region*, which contains a curve of the zero set. Second,
a *uniqueness region*, in which that zero set curve is unique. See the schematic in
Figure 9. The blue dot shows the initial approximate zero. The orange curve is
the zero set curve, which is guaranteed to lie within the accuracy region (the blue
region). Note that the approximate zero does not in general lie on the zero set. The
accuracy region is contained within the uniqueness region, shown in orange. The
uniqueness region is largest in phase space when the parameter is closest α^*. As the
parameter varies, the uniqueness region shrinks (meaning we have worse isolation).
The constructive implicit function theorem guarantees that the uniqueness region
is characterized by a linear norm condition, as depicted by the straight sides in the
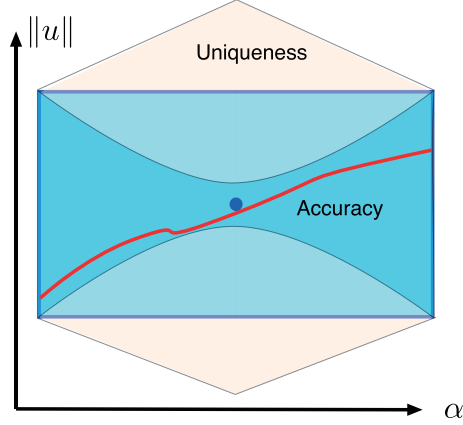
FIGURE 9. A schematic depiction of the constructive implicit function theorem. The theorem guarantees that under appropriate hypothesis, an approximate zero (blue dot) guarantees that within a uniqueness region (orange region) there is a curve in the zero set with a unique point at each fixed α value (red curve), and the this curve is located within an accuracy region (blue region). The uniqueness region contains the accuracy region. It is bounded in norm by straight lines, and the accuracy region is bounded in norm by parabolas.

schematic diagram. The accuracy region has best (i.e., smallest) accuracy when the parameter is near the parameter of the original point α^*. The accuracy region grows (meaning we have worse accuracy) with a quadratic norm condition. This is depicted schematically by its parabolic shape. We now state the formal theorem.

Theorem 3.1 (Constructive Implicit Function Theorem). *Let $\mathcal{P}$, $\mathcal{X}$, and $\mathcal{Y}$ be Banach spaces, suppose that the nonlinear operator $G : \mathcal{P} \times \mathcal{X} \to \mathcal{Y}$ is Fréchet differentiable, and assume the following hypotheses.*

(H1) *Small residual: There exists a pair $(\alpha^*, x^*) \in \mathcal{P} \times \mathcal{X}$ and a $\rho > 0$ such that*

$$\|G(\alpha^*, x^*)\|_{\mathcal{Y}} \leq \rho .$$

(H2) *Bounded derivative inverse: There exists a constant $K > 0$ such that*

$$\left\|D_x G(\alpha^*, x^*)^{-1}\right\|_{\mathcal{L}(\mathcal{Y}, \mathcal{X})} \leq K ,$$

where $\|\cdot\|_{\mathcal{L}(\mathcal{Y}, \mathcal{X})}$ denotes the operator norm in $\mathcal{L}(\mathcal{Y}, \mathcal{X})$.

(H3) *Lipschitz bound: There exist positive real constants L_1, L_2, ℓ_x, as well as $\ell_\alpha \geq 0$ such that for all $(\alpha, x) \in \mathcal{P} \times \mathcal{X}$ with $\|x - x^*\|_{\mathcal{X}} \leq \ell_x$ and $\|\alpha - \alpha^*\|_{\mathcal{P}} \leq \ell_\alpha$ we have*

$$\|D_x G(\alpha, x) - D_x G(\alpha^*, x^*)\|_{\mathcal{L}(\mathcal{X}, \mathcal{Y})} \leq L_1 \|x - x^*\|_{\mathcal{X}} + L_2 \|\alpha - \alpha^*\|_{\mathcal{P}} .$$

(H4) *Lipschitz-type bound: There exist positive real constants L_3 and L_4, such that for all parameters $\alpha \in \mathcal{P}$ with $\|\alpha - \alpha^*\|_{\mathcal{P}} \leq \ell_\alpha$ one has*

$$\|D_\alpha G(\alpha, x^*)\|_{\mathcal{L}(\mathcal{P}, \mathcal{Y})} \leq L_3 + L_4 \|\alpha - \alpha^*\|_{\mathcal{P}} ,$$

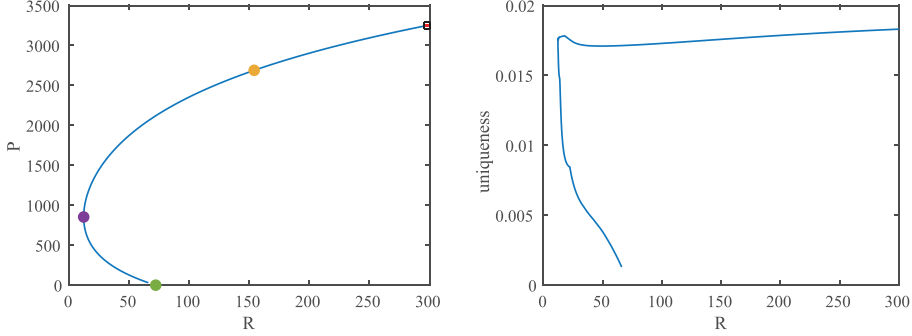*where ℓ_α is the constant that was chosen in (H3).*

FIGURE 10. Left, the validated bifurcation diagram of polyp density P as a function of the reproductive number R, along with the three validated bifurcation points. The blue curve consists of 5000 continuation steps, corresponding to 5000 linked boxes, for the preconditioned map with $\alpha = 0.8\ \delta_\alpha$. The initial validated box contains $(R, P) = (300, 3256)$, which is in the upper right corner of the bifurcation diagram, and the last validated box contains $(R, P) = (71.91, 1.493)$, which is close to the green transcritical bifurcation point. For comparison purposes, 4000 continuation steps for the unconditioned map are shown in red within the extremely small square region in the upper right-hand corner. Right, the norm of the uniqueness region of the solution. As the solution gets near the transcritical bifurcation at the origin, the uniqueness region gets smaller. This is expected, since there is no longer any uniqueness when the two branches of the solution curve meet.

Finally, suppose that

$$(3.1) \qquad\qquad 4K^2 \rho L_1 < 1 \qquad and \qquad 2K\rho < \ell_x .$$

Then there exist pairs of constants $(\delta_\alpha, \delta_x)$ with $0 \le \delta_\alpha \le \ell_\alpha$ and $0 < \delta_x \le \ell_x$, as well as

$$(3.2) \qquad 2KL_1\delta_x + 2KL_2\delta_\alpha \le 1 \qquad and \qquad 2K\rho + 2KL_3\delta_\alpha + 2KL_4\delta_\alpha^2 \le \delta_x ,$$

and for each such pair the following holds. For all $\alpha \in \mathcal{P}$ with $\|\alpha - \alpha^*\|_\mathcal{P} \le \delta_\alpha$ there exists a uniquely determined element $x(\alpha) \in \mathcal{X}$ with $\|x(\alpha) - x^*\|_\mathcal{X} \le \delta_x$ such that $\mathcal{G}(\alpha, x(\alpha)) = 0$. In other words, if we define

$$\mathcal{B}_\delta^\mathcal{X} = \{\xi \in \mathcal{X} \ : \ \|\xi - x^*\|_\mathcal{X} \le \delta\} \quad and \quad \mathcal{B}_\delta^\mathcal{P} = \{p \in \mathcal{P} \ : \ \|p - \alpha^*\|_\mathcal{P} \le \delta\} ,$$

then all points of the solution set of the equation $G(\alpha, x) = 0$ in the product set $\mathcal{B}_{\delta_\alpha}^\mathcal{P} \times \mathcal{B}_{\delta_x}^\mathcal{X}$ lie on the graph of the function $\alpha \mapsto x(\alpha)$.

In its classical form, the implicit function theorem is one of the central tools of bifurcation theory. Not only can it be used to establish the existence of small solution branches in nonlinear parameter-dependent equations, but by applying it as a tool to modified problems it can frequently be used to provide sufficient conditions for bifurcations. For example, the celebrated Crandall-Rabinowitz result [6] on bifurcation from a simple eigenvalue proves the existence of a bifurcating branch by

applying the implicit function theorem to a modification of the original nonlinear problem which removes the trivial solution. The constructive implicit function theorem can similarly be used as a tool for bifurcation analysis, yet in a computer-assisted proof setting. In fact, some first applications in this direction have already been provided in [12, 15]. With the current paper, we add two more applications.

More precisely, in the following we will be applying Theorem 3.1 in two different situations. In the remainder of this section, we apply it for branches of regular points. Through the introduction of a suitable extended system we can reformulate a validated step of pseudo-arclength continuation as an application of the constructive implicit function theorem to this extended system. Combined with suitable linking conditions, this establishes the existence of entire branches covered by slanted boxes.

In addition, in Section 4 we use Theorem 3.1 to validate bifurcation points. In that setting, and motivated by our earlier work [12], we will apply the theorem to an extended system without any parameter, as the parameter will be incorporated into the function for which we find a root. This parameter-free case means that we no longer need to find the Lipschitz constants relevant to the parameter variations, and we set these unused constants equal to zero.

3.2. **Continuation and an extended system.** To elaborate further on the validation of regular fixed points, the constructive implicit function theorem as stated in [15] only applies to a single region, validated at a single point. The same paper contains a version of this theorem for slanted boxes, using natural continuation in order to validate a branch of solutions by linking their validation sets to validate a larger portion of the branch. However, natural continuation leaves something to be desired in terms of efficiency. In this section, we develop a method of validation of bifurcation branches using pseudo-arclength continuation which allows for the direct application of the constructive implicit function theorem, and apart from Lipschitz estimates, only requires estimates at a single point in each box. This method is an improvement on the previous natural continuation method in that we can continue at limit points without having to change coordinates. The methods in this section apply for regular orbits along branches. In the next section, we will show how to adapt the constructive implicit function theorem in order to rigorously validate bifurcation points.

Before launching into further technicalities, we describe our results. Applying the pseudo-arclength continuation method to a preconditioned version of the coral model (preconditioning is discussed in Section 3.4 below), the resulting rigorously validated curve of fixed points is shown in Figure 10. While Figure 4 shows a similar picture, the distinction is that those points were found using numerical methods, and though we have a priori error estimates for these methods, we cannot guarantee existence or accuracy. In contrast, the points shown on the new figure are rigorously validated. The depicted points are an accurate indication of existing fixed points of the system, with known and validated accuracy and uniqueness region. In particular, the accuracy of our solutions is known individually for each separate box, and is always less than $1.453 \cdot 10^{-13}$, where the error in $x \in \mathbb{R}^{13}$ is measured in the maximum norm. Figure 10 shows the norm of the uniqueness for each separate box. The uniqueness shrinks when the curve approaches zero. This is not surprising,
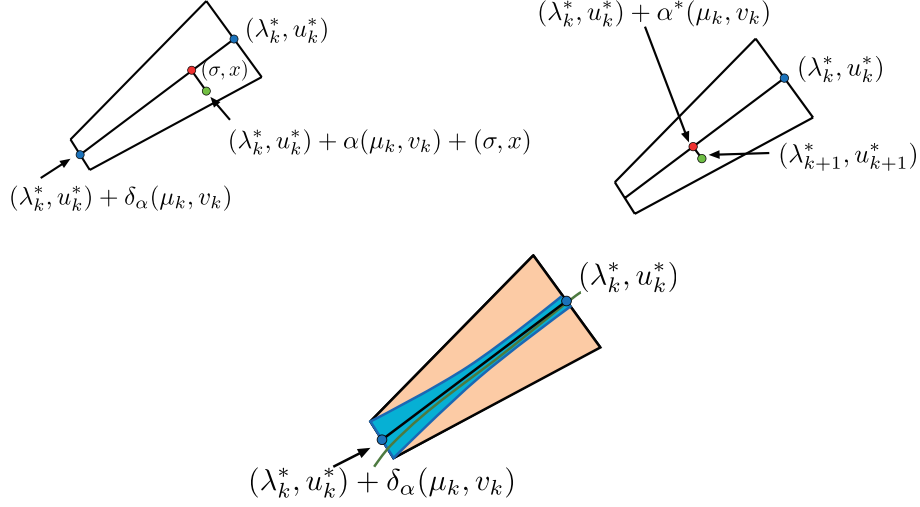
FIGURE 11. A schematic diagram of the the pseudo-arclength continuation method. Top left image: The result guarantees a uniqueness region for the zero set. This takes place in an adapted coordinate system, meaning that the box is slanted, but the uniqueness region is still bounded by straight lines. Since we only continue the curve in one direction, this figure only depicts the left half of the uniqueness region. The center line segment of this region is given by $(\lambda_k^*, u_k^*) + \alpha(\mu_k, v_k)$ for $0 \leq \alpha \leq \delta_\alpha$. At a fixed α value, we use Newton's method to find the next approximate zero along the line $(\lambda_k^*, u_k^*) + \alpha(\mu_k, v_k) + (\sigma, x)$, where (σ, x) denotes the vector pointing from $(\lambda_k^*, u_k^*) + \alpha(\mu_k, v_k)$ to the point $(\lambda_k^*, u_k^*) + \alpha(\mu_k, v_k) + (\sigma, x)$, and which is orthogonal to (μ_k, v_k). Top right image: After we fixed the value $\alpha = \alpha^*$, we label this next approximation $(\lambda_{k+1}^*, u_{k+1}^*)$. Bottom image: Inside the uniqueness region (orange) is an accuracy region (blue). The accuracy region is bounded by curves which are parabolic in norm in the adapted coordinate system.

since $x = 0$ is part of the zero set, putting a barrier on the size of the uniqueness region.

We now proceed with the constructive implicit function theorem for a validated pseudo-arclength continuation. In each continuation step we use continuation in a box with slanted sides, where the predictor step is performed along the middle of the box in the direction a specified vector (μ, v) (usually the estimated tangent to the zero set curve), and the corrector step uses a computation such as Newton's method to refine the estimate. This refinement is performed in a direction orthogonal to the predictor direction (μ, v). This is depicted in Figure 11. The left-hand image is a schematic diagram showing the box with its midline between two blue dots. The midline is the estimated tangent line in the direction (μ, v). Our validation gives us a maximum length of the box for which we can guarantee accuracy and uniqueness of the solution. The predictor, shown with a red dot, must be chosen

inside that box. The corrector, shown with a green dot is along an orthogonal line to the midline. The right-hand image shows the accuracy region in blue and the uniqueness region in orange. Note that the uniqueness region has large width near the starting point, and the accuracy region grows towards the ending point. In Figure 11, the uniqueness region for the box is approximately diamond shaped, whereas in Figure 12, the box is not only slanted but also has a uniqueness region which is asymmetric, more of a half-diamond. The half-diamond shape is in fact only half of the uniqueness box. In particular, as we are merely continuing in one direction, which in Figure 12 is to the left, we only show one side of the uniqueness box. The fact that we could continue to the right as well is not relevant for our continuation.

We now turn to the technical details of this approach. For this, we consider $F : \mathbb{R} \times U \to U$, where U denotes an arbitrary Euclidean space. Our goal is to implement pseudo-arclength continuation based on Theorem 3.1 to find branches of zeros of the nonlinear function F. For the specific application of this paper, we will consider $U = \mathbb{R}^{13}$ and $F(\lambda, x) = f(\lambda, x) - x$, where f is the coral model. Nevertheless, we use the more general notation based on F to indicate that these methods are general. In fact, the methods readily generalize to the Banach space setting as well. However, in this paper for convenience of notation we only consider the Euclidean space case. For any $(\lambda_0, u_0) \in \mathbb{R} \times U$, an approximate zero of F, and for a fixed direction vector $(\mu_0, v_0) \in \mathbb{R} \times U$, define $G : \mathbb{R} \times (\mathbb{R} \times U) \to \mathbb{R} \times U$ as follows

$$(3.3) \qquad G(\alpha, (\sigma, x)) = \begin{pmatrix} \mu_0 \sigma + v_0^t x \\ F(\lambda_0 + \alpha \mu_0 + \sigma, u_0 + \alpha v_0 + x) \end{pmatrix}.$$

The zeros of G as the parameter α varies correspond to the pseudo-arclength continuation solutions of F for a single continuation box. The first component of the function G guarantees that the pair (σ, x) is orthogonal to the direction (μ_0, v_0). As we will show in the next subsection, one can apply the constructive implicit function theorem from [15] directly to the extended function G and thereby perform rigorously validated pseudo-arclength continuation.

Since we will need them later, we close this subsection by explicitly stating the derivatives of G with respect to both the variables (σ, x) and with respect to the parameter α. These are respectively given by

$$(3.4) \qquad D_{(\sigma,x)} G(\alpha, (\sigma, x)) = \begin{pmatrix} A_{11} & A_{12} \\ A_{21} & A_{22} \end{pmatrix},$$

where

$$(3.5) \qquad \begin{aligned} A_{11} &= \mu_0, & A_{12} &= v_0^t, \\ A_{21} &= D_\lambda F(\lambda_0 + \alpha \mu_0 + \sigma, u_0 + \alpha v_0 + x), \\ A_{22} &= D_u F(\lambda_0 + \alpha \mu_0 + \sigma, u_0 + \alpha v_0 + x), \end{aligned}$$

as well as

$$(3.6) \qquad D_\alpha G(\alpha, (\sigma, x)) = \begin{pmatrix} B_1 \\ B_2 \end{pmatrix},$$

where

$$B_1 = 0 \,,$$

(3.7)
$$B_2 = D_\lambda F(\lambda_0 + \alpha\mu_0 + \sigma, u_0 + \alpha v_0 + x)\mu_0$$
$$+ D_u F(\lambda_0 + \alpha\mu_0 + \sigma, u_0 + \alpha v_0 + x)v_0$$

3.3. Pseudo-arclength validation theorem.

We are now in a position to start establishing assumptions under which we can validate a branch in the zero set of F using pseudo-arclength continuation. For this we need the following modified set of assumptions. For the purposes of this paper, we use the vector norm $\|(\alpha, x)\| = \max\{|\alpha|, \|x\|_U\}$ for all $(\alpha, x) \in \mathbb{R} \times U$, even though this could easily be modified.

(P1) We assume both

(3.8) $\|F(\lambda_0, u_0)\|_U \le \rho$ and $\|D_\lambda F(\lambda_0, u_0)\mu_0 + D_u F(\lambda_0, u_0)v_0\|_U \le \xi$.

(P2) Assume that there exists an explicit constant $K > 0$ which is a bound on the operator norm of the inverse of the matrix

$$D_{(\sigma,x)}G(0, (0,0)) = \begin{pmatrix} \mu_0 & v_0^t \\ D_\lambda F(\lambda_0, u_0) & D_u F(\lambda_0, u_0) \end{pmatrix} \,,$$

i.e., we suppose that

$$\left\| D_{(\sigma,x)}G(0, (0,0))^{-1} \right\|_{\mathcal{L}(\mathbb{R} \times U, \mathbb{R} \times U)} \le K \,.$$

For this, we interpret the matrix as a linear map on the product space $\mathbb{R} \times U$, and the operator norm is the norm in $\mathcal{L}(\mathbb{R} \times U, \mathbb{R} \times U)$.

(P3) Let M_1, M_2, M_3, and M_4 be Lipschitz constants such that for all pairs (λ, u) which satisfy $\|u - u_0\| \le d_u$ and $|\lambda - \lambda_0| \le d_\lambda$ we have the estimates

$$\|D_u F(\lambda, u) - D_u F(\lambda_0, u_0)\|_{\mathcal{L}(U,U)} \quad \le \quad M_1\|u - u_0\|_U + M_2|\lambda - \lambda_0| \,,$$

$$\|D_\lambda F(\lambda, u) - D_\lambda F(\lambda_0, u_0)\|_{\mathcal{L}(\mathbb{R},U)} \quad \le \quad M_3\|u - u_0\|_U + M_4|\lambda - \lambda_0| \,,$$

where as usual we will identify the norm in $\mathcal{L}(\mathbb{R}, U)$ with the norm $\|\cdot\|_U$ in the following.

We would like to point out that all of the above three conditions are formulated in terms of the nonlinear parameter-dependent function F and an approximate solution (λ_0, u_0) of the equation $F(\lambda, u) = 0$.

We now turn our attention to the extended system described by the operator G introduced in (3.3). It turns out that the above three assumptions are tailor-made to establish the hypotheses (H1) through (H4) from the constructive implicit function theorem for the mapping G. One can easily see that (P1) implies

$$\|G(0, (0,0))\|_{\mathbb{R} \times U} \le \rho \,,$$

i.e., hypothesis (H1) is satisfied. Furthermore, using the explicit derivative formulas from the end of the last subsection, the assumption (P2) immediately yields the estimate

$$\|D_{(\sigma,x)}G(0, (0,0))\|_{\mathcal{L}(\mathbb{R} \times U, \mathbb{R} \times U)} \le K \,,$$

which establishes (H2). It remains to show that (P3) furnishes the estimates in (H3) and (H4). For this, let ξ be defined as in (3.8), and define the four constants

$$
\begin{aligned}
L_1 &= \max(M_1 + M_3, M_2 + M_4) \,, \\
L_2 &= (M_1 + M_3)\|v_0\|_U + (M_2 + M_4)|\mu_0| \,, \\
L_3 &= \xi \,, \\
L_4 &= (M_1\|v_0\|_U + M_2|\mu_0|)\|v_0\|_U + (M_3\|v_0\|_U + M_4|\mu_0|)|\mu_0| \,.
\end{aligned}
$$

Then the constants L_1 through L_4 are the Lipschitz constants for the extended function G as required by (H3) and (H4). For this, first note that in view of (3.4) and (3.5) we have

$$
D_{(\sigma,x)}G(\alpha,(\sigma,x)) - D_{(\sigma,x)}G(0,(0,0)) =
$$

$$
\begin{pmatrix}
0 & 0 \\
D_\lambda F(w_1) - D_\lambda F(w_2) & D_u F(w_1) - D_u F(w_2)
\end{pmatrix},
$$

where $D_\lambda F$ and $D_u F$ are evaluated at $w_1 = (\lambda_0 + \alpha\mu_0 + \sigma, u_0 + \alpha v_0 + x)$ and $w_2 = (\lambda_0, u_0)$. Then one can readily see that (H3) follows from (P3) and the estimates

$$
\begin{aligned}
&\|D_{(\sigma,x)}G(\alpha,(\sigma,x)) - D_{(\sigma,x)}G(0,(0,0))\|_{\mathcal{L}(\mathbb{R}\times U, \mathbb{R}\times U)} \\
&\quad \leq \|D_u F(\lambda_0 + \alpha\mu_0 + \sigma, u_0 + \alpha v_0 + x) - D_u F(\lambda_0, u_0)\|_{\mathcal{L}(U,U)} \\
&\qquad + \|D_\lambda F(\lambda_0 + \alpha\mu_0 + \sigma, u_0 + \alpha v_0 + x) - D_\lambda F(\lambda_0, u_0)\|_{\mathcal{L}(\mathbb{R},U)} \\
&\quad \leq M_1(|\alpha|\|v_0\|_U + \|x\|_U) + M_2(|\alpha||\mu_0| + |\sigma|) \\
&\qquad + M_3(|\alpha|\|v_0\|_U + \|x\|_U) + M_4(|\alpha||\mu_0| + |\sigma|) \\
&\quad = (M_1 + M_3)\|x\|_U + (M_2 + M_4)|\sigma| \\
&\qquad + ((M_1 + M_3)\|v_0\|_U + (M_2 + M_4)|\mu_0|)|\alpha| \\
&\quad = L_1\|(\sigma,x)\|_{\mathbb{R}\times U} + L_2|\alpha| \,.
\end{aligned}
$$

Similarly, using (3.6) and (3.7) one can show that (H4) follows from (P1) and (P3), in combination with the inequalities

$$
\begin{aligned}
&\|D_\alpha G(\alpha,(0,0))\|_{\mathcal{L}(\mathbb{R},\mathbb{R}\times U)} \\
&\quad \leq \|D_\lambda F(\lambda_0, u_0)\mu_0 + D_u F(\lambda_0, u_0)v_0\|_U \\
&\qquad + \|D_u F(\lambda_0 + \alpha\mu_0, u_0 + \alpha v_0)v_0 - D_u F(\lambda_0, u_0)v_0\|_U \\
&\qquad + \|D_\lambda F(\lambda_0 + \alpha\mu_0, u_0 + \alpha v_0)\mu_0 - D_\lambda F(\lambda_0, u_0)\mu_0\|_U \\
&\quad \leq \xi + (M_1\|v_0\|_U + M_2|\mu_0|)|\alpha|\|v_0\|_U \\
&\qquad + (M_3\|v_0\|_U + M_4|\mu_0|)|\alpha||\mu_0| \\
&\quad = L_3 + L_4|\alpha| \,.
\end{aligned}
$$

Altogether, these estimates lead to the following result.

Theorem 3.2 (Pseudo-arclength continuation for a branch segment)**.** *Consider the fixed pairs (u_0, λ_0) and (v_0, μ_0) in $\mathbb{R} \times U$, let d_λ and d_u be two positive constants, and suppose that our hypotheses (P1), (P2), and (P3) are satisfied. Moreover, assume that both*

$$4K^2\rho < 1 \qquad and \qquad 2K\rho < d_u$$

hold. Then we can choose constants

$$0 < \delta_\alpha \leq d_\lambda \,, \quad 0 < \delta_u \leq d_u \,, \quad where \quad \delta_\alpha \|(\mu_0, v_0)\| + \delta_u \leq \min(d_u, d_\lambda) \,,$$

and such that

$$2KL_1\delta_u + 2KL_2\delta_\alpha \leq 1 \quad and \quad 2K\rho + 2KL_3\delta_\alpha + 2KL_4\delta_\alpha^2 \leq \delta_u \,.$$

Then for every $\alpha \leq \delta_\alpha$ there exists a unique (σ, x) in the zero set of G with $\|(\sigma, x)\| \leq \delta_u$.

These statements guarantee that there is a unique element of the zero set of F which lies on the hyperplane orthogonal to the center line in the slanted box between (λ_0, u_0) and $(\lambda_0 + \delta_\alpha\mu_0, u_0 + \delta_\alpha v_0)$ and passes through the point $(\lambda_0 + \alpha\mu_0, u_0 + \alpha v_0)$. This unique zero is given by $(\lambda_0 + \alpha\mu_0, u_0 + \alpha v_0) + (\sigma, x)$. Additionally, let

$$\delta_{\min} = 2K\rho \,.$$

Then for $\alpha = 0$ we can guarantee that the resulting pair in the zero of G is accurate within $\delta_{\min}$ of (λ_0, u_0), and this zero is unique within the set $\|(\sigma, x)\| \leq \min\{(2KL_1)^{-1}, d_u, d_\alpha\}$.

Proof. To show the theorem we follow the proof of [15, Theorem 5]. Aside from the changes in the Lipschitz constants which have already been derived before the formulation of the theorem, the only changes to the cited proof are due to the fact that for a fixed parameter of G, the values of both the parameter λ and the phase space value x of F can vary. Therefore, in order to guarantee that the Lipschitz estimates on F hold, we need to assure that for every $\alpha \leq \delta_\alpha$ and all $\|(\sigma, x)\| \leq \delta_u$ the norm $\|\alpha(\mu_0, v_0) + (\sigma, x)\|$ is bounded by both d_u and d_λ. This immediately leads to the additional constraints in the formulation of the theorem. $\qquad\square$

The above theorem gives a method for validating a branch segment of the zero set within a single slanted box. In practice we use this result successively to validate a whole solution branch. For each pair (λ_k^*, u_k^*), and for the approximate tangent (μ_k, v_k), we then define an extended function G_k, and validate a branch segment for F within the k-th box. For a fixed parameter value $\alpha_k \leq \delta_\alpha$, we then use Newton's method to find an approximate zero of F which is orthogonal to (μ_k, v_k), i.e., which is a zero of G_k. We abbreviate this approximate zero as $(\lambda_{k+1}^*, u_{k+1}^*)$, and can now repeat the entire process for the $(k + 1)$-st branch segment, see also Figure 12. What remains to be shown is that the successive validated boxes are linked, meaning that the branch segment in the k-th box and the branch segment in the $(k + 1)$-st box are on the same branch. That is, the accuracy region of the $(k + 1)$-st box has to be contained within the uniqueness region of the k-th box at the point α_k where we made the numerical estimate. We give the linking condition for two boxes in the next theorem.
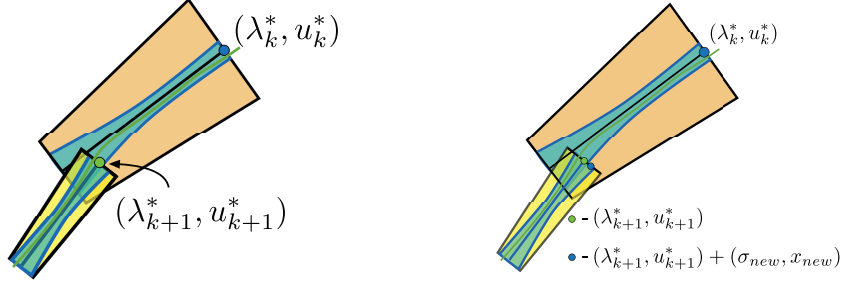
FIGURE 12. Left image: Associated with each successive approximation, there is a uniqueness region and an accuracy region. Right image: In order to guarantee that the k-th and $(k+1)$-st region enclose the same component of the zero set (the green curve), we must verify the linking condition. This requires that the accuracy curve of the $(k+1)$-st box at $\alpha = 0$ (such as the blue point on the upper edge of the $(k+1)$-st blue box) is contained in the uniqueness region of the k-th box (orange region).

Theorem 3.3 (Linking branch segments). *Let $\delta_{k+1,\min} = 2K_{k+1}\rho_{k+1}$ be the accuracy of the solution*

$$(\lambda_{k+1}^*, u_{k+1}^*) = (\lambda_k^* + \alpha_k \mu_k + \sigma^*, u_k^* + \alpha_k v_k + x^*) .$$

In order to guarantee that the two validated boxes are linked, we require the estimates

$$|\alpha_k| + \frac{\delta_{k+1,\min}}{\|(\mu_k, v_k)\|} < \delta_{k,\alpha} \qquad and \qquad |(\sigma^*, x^*)| + \delta_{k+1,\min} < \delta_{k,u} .$$

Proof. The accuracy of the $(k+1)$-st solution at $\alpha = 0$ is given by $\delta_{k+1,\min}$. That is, there exists a unique exact solution to $F = 0$ of the form

$$(\tilde{\lambda}, \tilde{u}) = (\lambda_{k+1}^* + \sigma_{new}, u_{k+1}^* + x_{new}) ,$$

where $\|(\sigma_{new}, x_{new})\| < \delta_{k+1,\min}$. In order to derive our linking condition we need to establish that this solution is contained in the uniqueness region of the k-th segment. We can therefore write

$$(\tilde{\lambda}, \tilde{u}) - (\lambda_k^*, u_k^*) = (\alpha_k + \alpha^+)(\mu_k, v_k) + (\sigma^* + \sigma^+, x^* + x^+) ,$$

where $(\sigma_{new}, x_{new}) = \alpha^+(\mu_k, v_k) + (\sigma^+, x^+)$, and (μ_k, v_k) is orthogonal to the vector (σ^+, x^+). Thus we have

$$\|\alpha^+(\mu_k, v_k) + (\sigma^+, x^+)\| < \delta_{k+1,\min} .$$

By the orthogonality of the two vectors, both the estimate $|\alpha^+|\|(\mu_k, v_k)\| < \delta_{k+1,\min}$ and the estimate $\|(\sigma^+, x^+)\| < \delta_{k+1,\min}$ are satisfied. In order to satisfy the linking condition, we have to require that both $|\alpha_k + \alpha^+| < \delta_{k,\alpha}$ and $\|(\sigma^* + \sigma^+, x^* + x^+)\| < \delta_{k,u}$ hold. This translates into the conditions

$$|\alpha_k + \alpha^+| \leq |\alpha_k| + \frac{\delta_{k+1,\min}}{\|(\mu_k, v_k)\|} < \delta_{k,\alpha} ,$$

as well as

$$\|(\sigma^* + \sigma^+, x^* + x^+)\| \leq \|(\sigma^*, x^*)\| + \delta_{k+1,\min} < \delta_{k,u} \; .$$

This completes the proof of the theorem.   □

3.4. **Preconditioning the coral map.** If we use the above method on the coral system, it is extremely slow to produce the bifurcation diagram. This is due to the different relative sizes of the components of the population and the parameter. We are able to significantly speed up the method by using preconditioning. In particular, for $k = 1, \ldots, d$ let

$$\tilde{f}_k(\tilde{R}, \tilde{u}) = \frac{f_k(100\tilde{R}, (s_1\tilde{u}_1, \ldots, s_d\tilde{u}_d))}{s_k} \; ,$$

where $s_1, \ldots, s_d$ are empirically determined positive scale constants. Then it is clear that if we write $(R, u) = (100\tilde{R}, (s_1\tilde{u}_1, \ldots, s_d\tilde{u}_d))$, then (R, u) is a fixed point of f if and only if $(\tilde{R}, \tilde{u})$ is a fixed point of the preconditioned map $\tilde{f}$. However, the map $\tilde{f}$ is better scaled in the sense that we expect all components and the parameter to be of the same order of magnitude. Therefore the pseudo-arclength continuation can be performed more efficiently. In particular, we find that the size of δ_α in the preconditioned version is (in comparable coordinates) around two orders of magnitude larger than those for the system without modification. This means that we are able to validate a much larger portion of the bifurcation diagram with the same number of continuation steps. Figure 10 shows 5000 continuation steps for the preconditioned case starting at $R = 300$ in the upper right corner, shown in blue. For comparison purposes, 4000 continuation steps are shown in red for the unmodified case. The bifurcation curve goes through a limit point and almost to $\|u\| = 0$ for the preconditioned case, but is hardly even a visible piece of red curve for the original unmodified map. A similar preconditioning is performed in the case of the bifurcation points, as described in the next section.

4. Validation of the bifurcation points

In this section, we discuss the validation of the bifurcation points. Namely, we have used a computer-assisted proof to validate the Neimark-Sacker bifurcation point, where the invariant circles form in Section 4.1 and the saddle-node bifurcation point in Section 4.2. In each case, to do so we create an extended system H such that $H = 0$ guarantees the needed conditions for a bifurcation point. We then apply the constructive implicit function theorem to H. In both cases, we use interval arithmetic for a separate computational validation of the extra transversality and nondegeneracy conditions. We also prove that there is a transcritical bifurcation point on the extinction axis. However, this last case does not require a computer-assisted proof for validation, since the calculations are simple enough for a closed form calculation.

4.1. **Validation of the Neimark-Sacker bifurcation point.** In Sections 2.4 and 2.5, we observed that at $(R, P) \approx (154.1, 2689)$, there is a change in stability of the fixed points, and for $R > 154.1$, typical initial conditions converge to populations which are oscillating in time. This is the behavior associated with a Neimark-Sacker bifurcation. In this section we detail the process of rigorous validation of the

Neimark-Sacker bifurcation point seen in the upper right corner of Figure 4. While this is the first time that a rigorous validation of a Neimark-Sacker bifurcation has been performed in this way, rigorous validation of Hopf bifurcations was performed in [18] in the context of ordinary and partial differential equations, but using a quite different method. Rather than considering conditions along a curve of fixed points or equilibria, instead the method used a validated continuation of periodic orbits with a renormalization technique, validating that there was a bifurcation of equilibria at the turning point of this invariant closed curve of solutions. Moreover, computer-assisted proofs were used in [5] to rigorously establish an invariant circle in a two-dimensional map, which is created via a Neimark-Sacker bifurcation. They do not, however, establish the bifurcation point itself directly. While it would be interesting to adapt their method to the coral model, this lies beyond the scope of the current paper.

We now proceed with our validation of the Niemark-Sacker bifurcation. As a first step, we state the standard theoretical Neimark-Sacker bifurcation theorem found in a bifurcation theory textbook. We then show how to adapt this classical result to create a rigorous computer-assisted bifurcation theorem.

Theorem 4.1 (Neimark-Sacker bifurcation point). *There is a Neimark-Sacker bifurcation for the coral system in (2.4) and (2.5) for the basic reproduction number $R_* \approx 154.1$ and with polyp population density $P_* \approx 2689$. The precise error bounds are stated in Table 2.*

The remainder of this subsection is devoted to the proof of this theorem. Our approach is to verify the classical conditions for a *Neimark-Sacker bifurcation*, as described for example in [11] — and which we briefly review in the following. Consider a smooth map $f : \mathbb{R} \times \mathbb{R}^d \to \mathbb{R}^d$. Furthermore, we begin by assuming the following two conditions:

(a) *Existence of a fixed point:* The map f has a fixed point at a specific parameter value, i.e., we assume that $f(\lambda_0, x_0) = x_0$.

(b) *Pair of imaginary eigenvalues on the unit circle:* The Jacobian matrix $D_x f(\lambda_0, x_0)$ has exactly one simple conjugate pair of imaginary eigenvalues on the unit circle. We denote these eigenvalues by $e^{\pm i\theta_0}$, for some angle $0 < \theta_0 < \pi$.

These two conditions have to be supplemented by another three transversality and nondegeneracy conditions, which will be stated in detail below. For this, however, we first need to introduce some additional notation.

Due to the implicit function theorem, as long as the Jacobian matrix in (b) does not have the eigenvalue 1, there exists a smooth curve of locally unique fixed points, which we denote by $(\lambda, x_0(\lambda))$. Moreover, we define

$$A(\lambda) = D_x f(\lambda, x_0(\lambda)) \,.$$

We would like to point out that in our application to the coral system, the rigorously established existence of the branch of fixed points as a side effect also implies that along the branch near the Neimark-Sacker point, the Jacobian matrix never has an eigenvalue 1.

Now let $p \in \mathbb{C}^d$ and $q \in \mathbb{C}^d$ denote the right eigenvectors of $A(\lambda_0)$ corresponding to $e^{i\theta_0}$ and $e^{-i\theta_0}$, respectively, and normalized in such a way that $\langle p, q \rangle = 1$, where the bracket notation denotes the usual complex scalar product $\langle p, q \rangle := \bar{p}^t q$. Finally, by Taylor's formula we can expand the function f in the form

$$(4.1) \qquad f(\lambda_0, x) - x_0 = A(\lambda_0)x + \frac{1}{2}B(x, x) + \frac{1}{6}C(x, x, x) + O(\|x\|^4) \,,$$

where B and C denote the second- and third-order derivative terms at the point (λ_0, x_0) in the form

$$B_i(y, z) = \sum_{j,k=1}^{d} \frac{\partial^2 f}{\partial x_j \partial x_k}(\lambda_0, x_0)y_j z_k$$

and

$$C_i(y, z, w) = \sum_{j,k,l=1}^{d} \frac{\partial^3 f}{\partial x_j \partial x_k \partial x_l}(\lambda_0, x_0)y_j z_k w_l \,.$$

After these preparations, we can now complete our description of the conditions needed for the Neimark-Sacker theorem:

(c) *Transversality condition:* Using the notation above, suppose that

$$\mathrm{Re}\left(e^{-i\theta_0}\left\langle p, \frac{dA}{d\lambda}(\lambda_0)q \right\rangle\right) \neq 0 \,.$$

(d) *Nondegeneracy condition I:* Suppose that

$$\theta_0 \neq \frac{\pi}{2} \quad \text{and} \quad \theta_0 \neq \frac{2\pi}{3} \,.$$

(e) *Nondegeneracy condition II:* Suppose that

$$Re\,(\ e^{-i\theta_0}(\langle p, C(q, q, \bar{q})\rangle + 2\langle p, B(q, (I - A)^{-1}B(q, \bar{q}))\rangle$$

$$+\langle p, B(\bar{q}, (e^{2i\theta_0}I - A)^{-1}B(q, q))\rangle)\ ) \quad \neq \quad 0 \,.$$

To summarize, the transversality condition implies that the pair of complex conjugate eigenvalues at λ_0 crosses the imaginary axis with nonzero speed. The first nondegeneracy condition indicates that the eigenvalues $e^{\pm i\theta_0}$ are not k-th roots of unity for $k = 1, \ldots, 4$. Since the proof of the Neimark-Sacker theorem is based on the Poincaré normal form theorem, this condition excludes resonances. Finally, the left-hand side of the second nondegeneracy condition gives the coefficient of the cubic term in the complex Poincaré normal form, and its sign distinguishes between a sub- and super-crital Neimark-Sacker bifurcation. For more details we refer the reader to the part of [11, Section 5.4] devoted to the Neimark-Sacker bifurcation.

Under the above conditions, the Neimark-Sacker theorem guarantees that a locally unique invariant closed curve bifurcates from the set of fixed points at the point (λ_0, x_0). As already mentioned, the type of bifurcation depends on the sign of the left-hand side of (e).

In order to create the validation version of this theorem, we use a suitable extended system to validate assumptions (a) and (b). After having established an existence and uniqueness result for this extended system, one can then validate conditions (c), (d), and (e) separately using interval arithmetic. For convenience,

R	λ	x_1	P
154.1	5.286	1794	2689

δ_1	δ_2	ρ	K
$1.473 \cdot 10^{-10}$	$1.220 \cdot 10^{-8}$	$6.166 \cdot 10^{-11}$	1.000

L_1	(c)	(d)	(e)
$4.097 \cdot 10^7$	$4.338 \cdot 10^{-2}$	46.85	$-1.21 \cdot 10^{-6}$

TABLE 2. Validation constants for the system (4.2) at the Neimark-Sacker bifurcation point. All values are written with four decimal places, unless less accuracy is known. For more efficient computation, we multiplied by a preconditioning matrix and determined the bounds ρ, K, and L_1. We selected a matrix close to the Jacobian matrix of H_{ns}, whose inverse was used as a preconditioner. The accuracy constant δ_1 and the isolation bound δ_2 were derived using ρ, K and L_1. For the three conditions (c), (d), and (e), which were checked separately after the validation involving H_{ns}, we used an interval arithmetic enclosure of the approximate solution with radius δ_1. Note that the angle in (d) is given in degrees.

we have converted the complex system into the following real system of equations. We are seeking zeros of the function $H_{ns} : \mathbb{R}^m \to \mathbb{R}^m$, which is defined as

$$(4.2) \qquad H_{ns}(x, \lambda, w, u, a, b) = \begin{pmatrix} f(\lambda, x) - x \\ D_x f(\lambda, x)w - aw + bu \\ D_x f(\lambda, x)u - bw - au \\ a^2 + b^2 - 1 \\ \|w\|^2 - 1 \\ \|u\|^2 - 1 \end{pmatrix}.$$

The first equation in the system is the fixed point condition. The second through fourth equations form the simple complex eigenvalue pair condition, where we write $e^{\pm i\theta_0} = a \pm ib$, and the eigenvectors p and q are given by $u \pm iw$, up to normalization. The last two equations are included to single out a locally unique eigenvector.

For a function of the form $f : \mathbb{R} \times \mathbb{R}^d \to \mathbb{R}^d$, we have $x \in \mathbb{R}^d$, $\lambda \in \mathbb{R}$, $u, w \in \mathbb{R}^d$, as well as $a, b \in \mathbb{R}$. Therefore, the extended system $H_{ns} : \mathbb{R}^m \to \mathbb{R}^m$ lives in dimension $m = 3d + 3$. In our numerical validation, we are working with a 13-dimensional system, implying that this extended system has dimension 42.

Using standard numerical methods, we obtained an approximate bifurcation point satisfying $H_{ns}(x, \lambda, w, u, a, b) = 0$, for the function H_{ns} in (4.2), and with values for R, λ, x_1, and P as stated in Table 2. Since H_{ns} is parameter free, we only seek rigorous solutions of the extended system in (4.2) which satisfy $H_{ns} = 0$ in $\mathbb{R}^{42}$. Thus we only need to verify the hypotheses of the constructive implicit function theorem which involve the values of ρ, K, L_1, and $\ell_x > 0$ at our computed approximation point. See also Theorem 3.1. Table 2 summarizes the constants found for the validation of the solution of system (4.2).

We obtain the bounds ρ and K by using interval arithmetic. While the bound ρ can be found in a straightforward way, the constant K cannot easily be found by using interval arithmetic to compute matrix inverses. Therefore, we first compute an approximate numerical inverse. However, we still need a bound on the exact inverse, and a bound on the accuracy of the approximate inverse. This is required in both the computation of K and twice when we verify condition (e). The required quantities can be determined using the following lemma. While we apply this lemma only for matrices, it is stated for the case of Banach spaces.

Lemma 4.2 (Inverse bounds). *Let A be a bounded linear operator between two Banach spaces, and let B be an approximate inverse of A. Assume further that*

$$\|I - BA\| \leq \rho_1 < 1 \qquad \text{as well as} \qquad \|B\| \leq \rho_2 \ .$$

Then A is one-to-one, onto, and we have both

$$\|A^{-1}\| \leq \frac{\rho_2}{1 - \rho_1} \qquad \text{and} \qquad \|B - A^{-1}\| \leq \frac{\rho_1 \rho_2}{1 - \rho_1} \ .$$

The bound on A^{-1} is due to a Neumann series argument, and the proof can be found in [15]. In addition, the second bound is a consequence of $\|B - A^{-1}\| \leq \|I - BA\| \|A^{-1}\|$.

Having described how the constants ρ and K can be estimated rigorously, we now turn our attention to the Lipschitz constant L_1. It can be determined using the mean value theorem for multivariate functions from the calculations in (4.3) below. For this, suppose that the function $H_{ns} : \mathbb{R}^m \to \mathbb{R}^m$ is differentiable and let $h_{ij}(x) = (\partial (H_{ns})_i / \partial x_j)(x)$. Then $h_{ij} : \mathbb{R}^m \to \mathbb{R}$, and we let $h : \mathbb{R}^m \to \mathbb{R}^{m \times m}$ denote the matrix-valued function with entries h_{ij}. Throughout our computations, we used the maximum norms for vectors x, and the induced matrix norm for matrices A. Recall that one then has $\|x\| = \|x\|_\infty = \max_{i=1,\ldots,m} |x_i|$, as well as $\|A\| = \|A\|_\infty = \max_{i=1,\ldots,m} \sum_{j=1}^m |A_{ij}|$. After these preparations, the mean value theorem implies

$$|h_{ij}(x) - h_{ij}(y)| \leq \max_{c \in D} \|\nabla h_{ij}(c)\|_1 \|x - y\| \ ,$$

where D denotes the line segment between the points x and y. Together with the definition of the functions h_{ij} one further obtains

$$
\begin{aligned}
|h_{ij}(x) - h_{ij}(y)| &\leq \max_{c \in D} \left\| \left(\frac{\partial^2 (H_{ns})_i}{\partial x_1 \partial x_j}(c), \ldots, \frac{\partial^2 (H_{ns})_i}{\partial x_n \partial x_j}(c) \right) \right\|_1 \|x - y\| \\
&\leq m \max_{c \in D, \, k=1,\ldots,m} \left| \frac{\partial^2 (H_{ns})_i}{\partial x_k \partial x_j}(c) \right| \|x - y\| \ .
\end{aligned}
$$

This finally furnishes

$$
\begin{aligned}
\|h(x) - h(y)\| &= \max_{i=1,\ldots,m} \sum_{j=1}^m |h_{ij}(x) - h_{ij}(y)| \\
(4.3) \qquad &\leq \max_{i=1,\ldots,m} \sum_{j=1}^m \left(m \max_{c \in D, \, k=1,\ldots,m} \left| \frac{\partial^2 (H_{ns})_i}{\partial x_k \partial x_j}(c) \right| \right) \|x - y\| \ .
\end{aligned}
$$

The factor in front of $\|x-y\|$ on the right-hand side is then the Lipschitz constant L_1, and it can be determined via interval arithmetic and automatic differentiation.

Altogether, our rigorous computer-assisted proof of Theorem 4.1 can be summarized as follows. After completing the validation of the conditions that guarantee that the constructive implicit function theorem holds, we are able to verify the accuracy and uniqueness regions for the bifurcation point. In addition, we can use Intlab [13] to rigorously show that the Jacobian matrix $D_x f(\lambda_0, u_0)$ has in fact only two eigenvalues on the unit circle, by verifying that the remaining eleven eigenvalues all lie inside the unit disk. This implies that a bifurcation occurs within the specified error of the approximate bifurcation point. We then verify that this bifurcation is indeed a Neimark-Sacker bifurcation by showing that conditions (c), (d), and (e) hold using interval arithmetic on these conditions. Here are a few remarks which give a more detailed explanation:

- For each condition, we show that the interval containing the exact answer does not contain zero for (c) and (e), and does not contain any of the avoided angles for (d).
- While we are able to work with real-valued quantities a, b, u, v in the initial calculations of parts (a) and (b), we must switch to the complex case to verify the extra conditions (c), (d), (e), and we normalize the complex vectors p and q using the normalization condition $\langle p, q \rangle = 1$.
- We need to be able to guarantee that all three conditions are satisfied for the entire accuracy region. Therefore we evaluate these conditions on an interval vector whose midpoint is the approximate bifurcation point, and whose radius is δ_1. That is, every component of the vector is an interval. The actual computed values of the conditions (c)-(e) are intervals, but the values given in Table 2 are the worst-case scenario values. Even with the interval calculations, conditions (c) and (d) are known to more than four significant digits, but condition (e) is only known to three digits of accuracy.

This completes the proof of Theorem 4.1.

4.2. **Validation of the saddle-node bifurcation point.** In this section, we use a computer-assisted proof to show that there is a saddle-node bifurcation point in the coral model. The precise result can be stated as follows.

Theorem 4.3 (Saddle-node bifurcation point)**.** *The coral model in (2.4) and (2.5) has a saddle-node bifurcation point near the basic reproduction number $R_* \approx 12.28$, which corresponds to the parameter value $\lambda_* \approx 0.4213$, and for polyp population density $P_* \approx 853.4$. The precise error bounds are stated in Table 3.*

As in the previous subsection, the remainder of the present one is devoted to the verification of this theorem via computer-assisted rigorous methods. In order to establish the theorem, we need to verify the following conditions from the *classical saddle-node bifurcation theorem*, see for example [11]. Let $f : \mathbb{R} \times \mathbb{R}^d \to \mathbb{R}^d$ be a smooth mapping. Furthermore, assume the following four conditions:

(a) *Existence of a fixed point:* The map f has a fixed point at a specific parameter value, i.e., we assume that $f(\lambda_0, x_0) = x_0$.

R	λ	x_1	P	δ_1	δ_2
12.28	0.4213	569.5	853.4	$3.306 \cdot 10^{-12}$	$4.015 \cdot 10^{-7}$
ρ	K	L_1	(c)	(d)	
$1.653 \cdot 10^{-12}$	1	$1.245 \cdot 10^6$	-353.4	$-9.924 \cdot 10^{-4}$	

TABLE 3. Validation constants for the extended system in (4.4) at the saddle-node bifurcation point. All values are written up to four decimal places. For more efficient computation, we multiplied by a preconditioning matrix and obtained the bounds ρ, K, and L_1. We selected a matrix close to the Jacobian matrix of H_{sn}, whose inverse was used as a preconditioner. The accuracy constant δ_1 and the isolation bound δ_2 were derived using ρ, K, and L_1. For the two conditions (c) and (d), which were checked separately after the validation involving H_{sn}, we used an interval arithmetic enclosure of the approximate solution with radius δ_1.

(b) *Simple eigenvalue 1:* The Jacobian matrix $D_x f(\lambda_0, x_0)$ has a simple eigenvalue of 1. Let p and q denote the corresponding left and right eigenvectors, and suppose they are normalized to satisfy $p^t q = 1$.

(c) *Transversality condition:* Using the above notation we assume

$$p^t D_\lambda f(\lambda_0, x_0) \neq 0 .$$

(d) *Nondegeneracy condition:* Now let $A(\lambda_0) = D_x f(\lambda_0, x_0)$, and consider the expansion of f given in (4.1). Then we suppose further that

$$p^t B(q, q) \neq 0 .$$

Then the classical saddle-node bifurcation theorem guarantees a saddle-node bifurcation at the pair (λ_0, x_0).

In order to validate our bifurcation point using this theorem, we use again an extended system of the form $H_{sn} = 0$ to validate conditions (a) and (b), and then we verify conditions (c) and (d) separately afterwards. This time, the extended mapping H_{sn} is a map $H_{sn} : \mathbb{R}^{27} \to \mathbb{R}^{27}$, and it is defined as

$$(4.4) \qquad H_{sn}(x, v, \lambda) = \begin{pmatrix} f(\lambda, x) - x \\ D_x f(\lambda, x)v - v \\ \|v\|^2 - 1 \end{pmatrix} .$$

In order to validate (c), and (d), we use interval arithmetic for both of these conditions, and show that 0 does not lie in the interval containing the resulting answer. Note that the vector q is just a multiple of v, and p can be found in a verified way using Intlab [13]. The summary of the constants of this validation process is given in Table 3. This computer-assisted proof is quite similar to the one used for the Neimark-Sacker bifurcation in the last subsection, and therefore we do not give any more elaboration on the technique used to compute these values. This completes the proof of Theorem 4.3.

4.3. **Validation of the transcritical bifurcation point.** We close this section by showing that there is indeed a transcritical bifurcation on the trivial solution curve, i.e., the extinction curve. This time, it is not necessary to perform a computer-assisted proof, as the bifurcation can be established directly by hand.

Theorem 4.4 (Transcritical bifurcation point). *For the coral population model in (2.4) and (2.5) there exists a transcritical bifurcation point for basic reproduction number $R_* = c_2/c_1 \approx 72.22$, which corresponds to the parameter value $\lambda_* = R_*/(b \cdot a)$ and to $x_* = 0 \in \mathbb{R}^{13}$. Recall that the constants c_1 and c_2 were introduced in (2.2), and the vectors a and b were defined in (2.6) and the following paragraph.*

Proof. It is clear from the model that $x = 0$ is a fixed point for all values of the parameter λ. Furthermore, one can easily show that

$$\det(D_x f(\lambda, 0) - I) = \lambda - \frac{c_2}{c_1(b \cdot a)} \ .$$

Therefore, the Jacobian matrix of $f(\lambda, \cdot)$ at the origin has a simple eigenvalue of 1 if and only if λ equals

$$\lambda_* = \frac{c_2}{c_1(b \cdot a)} \ .$$

Now denote the right and left eigenvectors of $D_x f(\lambda_*, x_*)$ by v and w, respectively. One can show directly that $v = a$ defined in (2.6), and w is such that

$$w_1 = b \cdot a \ , \quad w_d = b_d \ , \quad \text{and} \quad w_k = b_k + S_k w_{k+1} \quad \text{for} \quad k = 2, \ldots, d-1 \ .$$

Then in order to establish the transcritical bifurcation, two nondegeneracy conditions have to be verified. Since we have $w^t D_\lambda f(\lambda_*, x_*) = 0$, one first has to show that

$$w^t D_{x\lambda} f(\lambda_*, x_*) v = \frac{(b \cdot a) c_1}{c_2} w^t b$$

is nonzero, which is clearly satisfied since all the terms of b and w are non-negative, and contains terms of the form b_k^2 (which are strictly positive for each nonzero b_k).

Second, we need to show that $w^t D_{xx} f(\lambda_*, x_*)[v, v] \neq 0$. Since only the first component of f, which we call f_1, is nonlinear, one merely needs to consider the second derivative of this component function. We get the following formula.

$$D_{xx} f_1(\lambda_*, x_*)[v, v] = \frac{2(\beta - \alpha)}{\Omega} \sum_{k=2}^{d} p_k a_k.$$

By looking at the corresponding parameter values, this value is also nonzero, and therefore the second nondegeneracy condition holds. This completes the proof of the theorem. □

5. Conclusion

In this paper, we have considered an age-structured population model for red coral populations with a parameter of fitness. When the fitness increases sufficiently, a set of stable invariant closed curves of oscillating orbits form, and these stable curves persist for large values of the fitness parameter. It is not surprising that for small fitness parameters, solutions limit to extinction, but we see that even for

large fitness, populations become extremely vulnerable, as they limit to oscillation spending long period of time near extinction.

The coral population model has a curve of fixed points containing a Neimark-Sacker, saddle-node, and transcritical bifucation point. We develop new methods based on previous computer-assisted proof methods and use these methods to validate the branch of fixed points, and the three bifurcation points.

Acknowledgments

References

[1] R. Aubourg, *Red coral in the Mediterranean sea*, Wikimedia Commons, 2 November 2017.

[2] S. Beslin, D. Baney and V. de Angelis, *Small denominators: No small problem*, Mathematics Magazine **71** (1998), 132–138.

[3] L. Bramanti, M. Iannelli and G. Santangelo, *Mathematical modelling for conservation and management of gorgonians corals: youngs and olds, could they coexist?*, Ecological Modelling **220** (2009), 2851–2856.

[4] L. Bramanti, G. Magagnini, L. D. Maio and G. Santangelo, *Recruitment, early survival and growth of the Mediterranean red coral Corallium rubrum (L 1758), a 4-year study*, Journal of Experimental Marine Biology and Ecology **314** (2005), 69–78.

[5] M. J. Capinski, E. Fleurantin and J. D. Mireles James, *Computer assisted proofs of two-dimensional attracting invariant tori for odes*, Discrete and Continuous Dynamical Systems, Series A, 2020, To appear.

[6] M. G. Crandall and P. H. Rabinowitz, *Bifurcation from simple eigenvalues*, Journal of Functional Analysis **8** (1971), 321–340.

[7] S. Das, C. Dock, Y. Saiki, M. Salgado-Flores, E. Sander, J. Wu and J. Yorke, *Measuring quasiperiodicity*, Europhysics Letters **114** (2016): 40005.

[8] P. Géry, *Corallium rubrum (Linnaeus, 1758) - Banyuls-sur-Mer, Sec de Rédéris: 08/84*, Wikimedia Commons, 31 July 2011.

[9] W. J. F. Govaerts, *Numerical Methods for Bifurcations of Dynamical Equilibria*, Society for Industrial and Applied Mathematics (SIAM), Philadelphia, PA, 2000.

[10] H. B. Keller, *Lectures on numerical methods in bifurcation problems*, in: Tata Institute of Fundamental Research Lectures on Mathematics and Physics, vol. 79, Published for the Tata Institute of Fundamental Research, Bombay; by Springer-Verlag, Berlin, 1987. With notes by A. K. Nandakumaran and Mythily Ramaswamy.

[11] Y. A. Kuznetsov, *Elements of Applied Bifurcation Theory*. Springer-Verlag, New York, second edition, 1998.

[12] J.-P. Lessard, E. Sander and T. Wanner, *Rigorous continuation of bifurcation points in the diblock copolymer equation*, Journal of Computational Dynamics **4** (2017), 71–118.

[13] S. M. Rump, *INTLAB - INTerval LABoratory*, in: Developments in Reliable Computing, T. Csendes (ed), Kluwer Academic Publishers, Dordrecht, 1999, pp. 77–104.

[14] E. Sander and J. D. Meiss, *Birkhoff averages and rotational invariant circles for area-preserving maps*, Physica D **411** (2020): 132569.

[15] E. Sander and T. Wanner, *Validated saddle-node bifurcations and applications to lattice dynamical systems*, SIAM Journal on Applied Dynamical Systems **15** (2016), 1690–1733.

[16] E. Sander and T. Wanner, *Equilibrium validation in models for pattern formation based on Sobolev embeddings*, Discrete and Continuous Dynamical Systems, Series B, 2020, To appear.

[17] G. Santangelo, L. Bramanti and M. Iannelli, *Population dynamics and conservation biology of the over-exploited Mediterranean red coral*, Journal of Theoretical Biology **244** (2007), 416–423.

[18] J. B. van den Berg, J.-P. Lessard and E. Queirolo, *Rigorous verification of Hopf bifurcations via desingularization and continuation*, arXiv:2006.13373 [math.DS], 2020.

[19] T. Wanner, *Computer-assisted equilibrium validation for the diblock copolymer model*, Discrete and Continuous Dynamical Systems, Series A **37** (2017), 1075–1107.

[20] T. Wanner, *Computer-assisted bifurcation diagram validation and applications in materials science*, Proceedings of Symposia in Applied Mathematics **74** (2018),123–174.

S. Kamimoto
Department of Mathematical Sciences, George Mason University, Fairfax, VA 22030, USA
  E-mail address: skamimot@gmu.edu

H. K. Kim
School of Mathematics, University of Minnesota, Minneapolis, MN 55455, USA
  E-mail address: kim00486@umn.edu

E. Sander
Department of Mathematical Sciences, George Mason University, Fairfax, VA 22030, USA
  E-mail address: esander@gmu.edu

T. Wanner
Department of Mathematical Sciences, George Mason University, Fairfax, VA 22030, USA
  E-mail address: twanner@gmu.edu